

FEM Analyses for the Design and Modeling of a Novel Flywheel Energy Storage System Assisted by Integrated Magnetic Bearing

C. Zhang, *Student Member, IEEE*, P. Wu, *Student Member, IEEE* and K. J. Tseng, *Senior Member, IEEE*

Centre for Advanced Power Electronics, Nanyang Technological University
Blk S2, Nanyang Avenue, Singapore 639798, Republic of Singapore

Abstract—A compact and efficient flywheel energy storage system is proposed in this paper. The system is assisted by integrated mechanical and magnetic bearings, the flywheel acts as the rotor of the drive system and is sandwiched between two disk type stators to save space. The combined use of active magnetic bearings, mechanical bearings and axial flux PM synchronous machine assists the rotor-flywheel to spin and remain in magnetic levitation in the vertical orientation, while constrains the other four degrees of freedom in radial directions mechanically. The mathematical model of the proposed system has been derived. Three-dimensional finite element method is applied for studying the performances and verifying the mathematical model of the system. The analysis results support the feasibility of the system.

I. INTRODUCTION

IN modern power industries, with the advances of high strength and light weight composite material, control technology and power electronics, the Flywheel Energy Storage System (FESS) is becoming a viable alternative to traditional chemical battery systems, with its advantages such as higher energy storage density, lower risk of overcharge and over-discharge, easier detection of the depth of discharge, operation over a wider temperature range, longer lifespan and environmental friendliness [1]-[4]. As a result, FESS is now considered a promising technology for many applications including spaceflight, transportation, power industry, military, and building services.

In general, a flywheel energy storage system is composed of a flywheel, magnetic or mechanical bearings that support the flywheel, a motor-generator to drive the flywheel and inter-convert the mechanical energy and electrical energy, control and power electronic devices, and touchdown bearings. This separate driving motor-generator in addition to magnetic bearings makes the rotor long and apt to produce bending vibrations. And the large motor-bearing system makes it difficult for miniaturization [5]. To overcome these problems, a self-bearing permanent magnet motor is introduced. The motor combines magnetic bearing and motoring functionality into a single magnetic actuator. Such designs can reduce the overall length of a motor because less mechanical bearings are required, thus increasing power density, reducing weight, and lowering susceptibility to rotor dynamic vibrations [6].

As shown in Fig. 1, there are three directions along x , y and z axes within the flywheel, such that six degrees-of-freedom (DOF) which are the displacement and rotation of every axis

should be controlled with the help of mechanical or magnetic bearings. Mechanical bearings have the advantages of simple structure and easy operation, but the frictional loss and thereby, the use of lubrication should always be taken into consideration. Especially, the friction occurring on the bearing which is along the direction of the gravity, i.e., the direction along z axis in Fig. 1, is much greater than those in the other directions. For this reason, it is not practical to use mechanical bearings along this axis, while for the other axes, they can still be tolerated. Active magnetic bearings have many advantages over the conventional bearings. Such benefits include higher energy efficiency, lower wear, longer lifespan, absence of need of lubrication and mechanical maintenance, and wider range of operating temperatures. There are many studies concerning magnetic bearings, but most of them treat the bearing in which at least five DOF of the object are controlled. Since the control of each DOF requires a sensor, an actuator and a controller, the entire system becomes complex in terms of the design of its mechanical/ electrical part and the control system [7]. Considering this, this paper presents a new concept of magnetic bearing, in which only 2 DOF of an axis, namely, the translation and rotation along and about axial directions respectively, are actively controlled. The motions in other directions are entirely restricted by mechanical bearings. The combined use of active magnetic bearings and mechanical bearings can cut down the complexity of control and make the system more stable, viable and cost-effective.

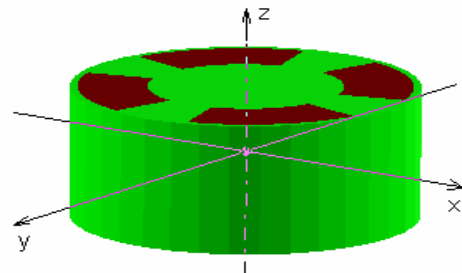


Fig. 1. Three motion directions of flywheel.

Currently, axial flux permanent magnet motors (AFPM) used in many applications have become an appealing research field [8] [9]. They have several unique features such as high efficiency, high power and torque densities, low rotor losses and small magnetic thickness. However, the disadvantage is that the distributed windings have end-windings of significant length compared to the active part of the coil conductors. This

obviously results in poor machine performance, as a significant part of the machine copper (i.e., more than 50% of the total in most machine designs) is producing heat but no torque [10]. Concentrated windings can solve this problem. Furthermore, they have simpler design, easier arrangement and higher efficiency.

The finite element method (FEM) has proved to be particularly flexible, reliable and effective in the analysis and synthesis of power-frequency electromagnetic and electromechanical devices [11] [12]. The FEM can analyze PM circuits of any shape and material. A remarkable advantage of FEM analysis over other approaches to analysis of PM motor is the inherent ability to calculate accurately armature reaction effects, electromagnetic force and torque.

In this paper, a novel flywheel energy storage system assisted by integrated magnetic bearing is proposed. The motor and generator are combined to be a single machine and the flywheel functions as the rotor in order to save space. Mechanical bearings are used to restrict the displacement and rotation along radial directions, and the displacement and rotation along axial direction are controlled by active magnetic bearings. The structure and electromagnetic design of the proposed system is presented along with the mathematical model. 3D FEM analyses are implemented to verify the mathematical model and support the feasibility of the system. Analysis results have been obtained and are presented in this paper.

II. CONSTRUCTION AND GEOMETRY OF THE PROPOSED SYSTEM

A. Configuration of the Entire System

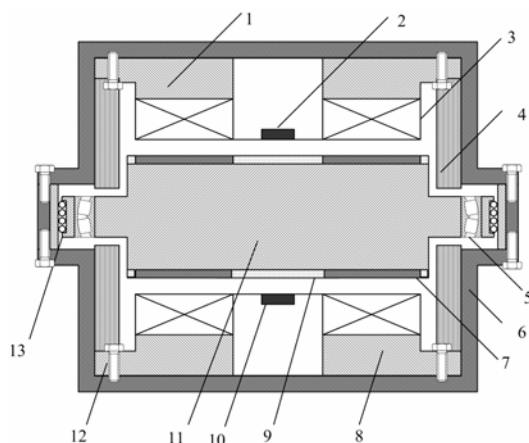


Fig. 2. Cross-sectional diagram of the proposed system.

Fig.2 shows the cross-sectional diagram of the proposed flywheel energy storage system. Its components are listed in Table I. Items 1 and 8 are the upper and lower stators fixed on the system housing which is designed to dissipate radial kinetic energy from any rotor debris and ensure safety in the event of mechanical failure. Axial flux permanent magnet synchronous motor is implemented to drive the flywheel which is also functioning as a rotor.

TABLE I
COMPONENTS OF THE PROPOSED SYSTEM

Item Number	Item Name
1	Upper stator
2	Position sensor
3	Stator windings
4	Touchdown bearings
5	Rotational ball bearing
6	System housing
7	Rotor permanent magnets
8	Lower stator
9	Non-magnetic material guard ring
10	Rotation sensor
11	Flywheel-rotor
12	Fasteners
13	Sliding ball bearing

Mechanical rotational ball bearings are mounted on the outer rim of the rotor to constrain its radial motion and assist the rotation of the flywheel/rotor. This arrangement makes the structure very compact without using the shaft. But the large diameter of the bore of the mechanical bearing limits the maximum speed. By using fluid-film bearings, the DN value (bore diameter mm \times speed rpm) can reach 3,000,000 [13]. That means the maximum speed is less than 20,000 rpm when the bore diameter is 150 mm. In higher speed flywheel system, two mechanical bearings can be mounted at the ends of the shaft which is fixed in the middle of the rotor. With this arrangement, the speed may reach up to 60,000 rpm and above.

The axial motion can be realized with the aid of 4 sliding ball bearings installed orthogonally on the rim of the rotational ball bearing. Non-contact eddy current displacement sensor and photo electrical sensor are set in the hollow center of the two stators to detect the displacement and angular position along z-axis when the rotor spins, (items #2 and #10 in Fig. 2). Touchdown bearings are necessary during starting operation or in the event of magnetic bearings failure. The touchdown bearings shall be mounted against the outer rim of the rotor. During normal operation, there is a less than 0.5 mm air-gap between all rotor surfaces and the touchdown bearings, thus achieving a mechanically contact-less environment.

B. Basic Features of the Proposed System

Fig.3 shows the basic features of the proposed system. The motor and generator with disk-type geometry are combined into a single electric machine as shown in Fig.3 (a). The rotor doubles as the flywheel and is sandwiched between two disk-type stators. This design maximizes the torque production area of the disk-type rotor.

As shown in Fig.3 (b), each of the upper and lower stators carries a set of three-phase copper windings to be fed with sinusoidal currents; concentrated windings are implemented to reduce the power loss. If distributed windings are used, the winding-ends will span half the circumference of the rotor. The ends are much longer compared to the effective parts of coil conductors, and the copper loss of the windings will thus be larger. In this particular design, there are 6 coils, each of which surrounds a stator tooth. The distribution of three phases and directions of the three-phase currents at a particular instance are

shown in Fig. 4. Besides improved efficiency, simple structure and easy installation of the stator winding can also be realized in this design.

Permanent magnets are mounted on both surfaces of the rotor, as shown in Fig.3 (c). The arrangement of these PMs and the magnetic flux flowing in the motor are depicted in Fig.4. PMs are settled in opposite directions in upper and lower rotor faces, so that they would attract each other and increase the total flux in the magnetic circuits.

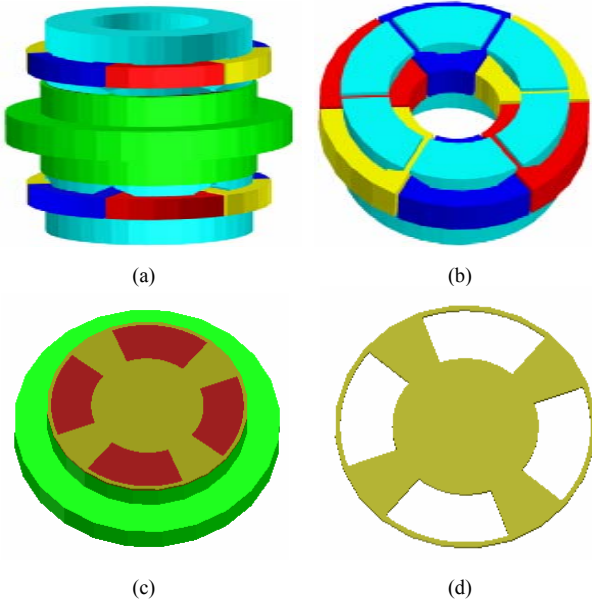


Fig. 3. Basic parts of the proposed flywheel system. (a) Stator-rotor Assembly. (b) Stator Windings. (c) Rotor-flywheel. (d) Non-magnetic guard ring.

A guard ring made of high strength non-magnetic material is used to assist the PMs in resisting the centrifugal force, as shown in Fig.3 (d).

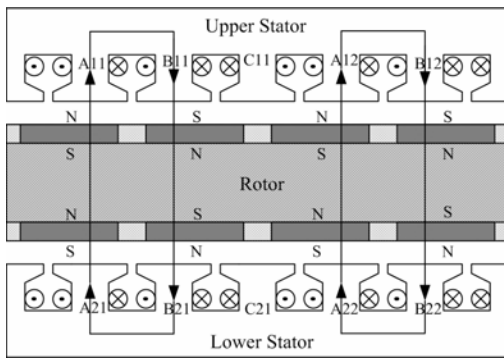


Fig. 4. Motor development structure and 2D flux pattern.

Magnetic bearings can be realized by using attractive forces. The interaction between the stator and rotor fields produces an axial force that makes the rotor and stator attract each other. The currents of each stator can be independently adjusted to control the net forces on the rotor and keep it in the middle of

the two stators. The net force along the axial axis can be obtained as

$$F = F_2 - F_1 \quad (1)$$

Where F_1 is the force between the lower stator and rotor; F_2 is the force between the upper stator and rotor.

The motor-generator is equivalent to two motors, the total torque T can be written as

$$T = T_1 + T_2 \quad (2)$$

Where T_1 and T_2 are torques generated by the upper and lower motor respectively.

C. Dimensions of the Motor

The size of axial flux motor can be transformed to that of an equivalent sized radial machine by the following formulas

$$D = \frac{D_o + D_i}{2} \quad (3)$$

$$L = \frac{D_o - D_i}{2} \quad (4)$$

where D_o and D_i are the outer and inner diameters of the axial flux disk-type motor, D and L are the inner diameter and length of the equivalent radial machine. Maximum torque is produced when $K_R = D_o / D_i = \sqrt{3}$.

From output equation of the motor, we can get

$$D^2 L = \frac{Q}{C_0 n_s} \quad (5)$$

and then, we can obtain

$$D_o = \sqrt[3]{\frac{8QK_R^3}{(K_R + 1)^2 (K_R - 1) C_0 n_s}} \quad (6)$$

where C_0 is the output coefficient, Q is the rating of machine in kVA, n_s is the rated speed in r.p.s.

$$C_0 = 11B_{gav}AK_w \times 10^{-3}, Q = \frac{K_E P_N}{\eta_N \cos \phi_N} \quad (7)$$

where B_{gav} represents the average flux density over the air-gap of the machine, also known as magnetic loading; A is the electric loading; K_w is the winding factor; P_N , η_N and $\cos \phi_N$ represent rated power, efficiency and power factor respectively; K_E is the ratio between induced EMF and the voltage. In this design, $K_E = 0.905$.

Minimum length of air-gap is set by mechanical constraints and is unlikely to be less than 0.3 mm. Magnets' depth should generally be reduced to a minimal value so as to minimize the cost of the magnets. Manufacturing restrictions make it difficult to have magnets thinner than 2.0mm. In this design, l_g is selected as 0.5 mm, and l_m is set to be 2.5 mm.

According to the design requirement data shown in Table II, the motor design results can be obtained as in Table III. This is just a test design to verify the feasibility of the system structure and the correctness of the mathematical model. So the rated

speed is only selected to be 1500 rpm.

TABLE II
DESIGN REQUIREMENT DATA

Rated power	1 kVA
Phase current, rms	1.85 A
Power factor	0.9
Efficiency	0.9
Rated speed	1500 rpm
Frequency	50 Hz
Slot fill factor	0.4
Remanent flux density	1.23 T
Magnet recoil permeability	1.05
Carter's factor	1.05

TABLE III
DESIGN GEOMETRICAL DATA

No. of pole pairs	2
No. of slots	6
Outer diameter of stator	130 mm
Inner diameter of stator	76 mm
Permanent magnets length	2.5 mm
Air gap length	0.5 mm
Slot width	28 mm
Slot depth	22 mm
Stator yoke thickness	18 mm
Rotor core thickness	60 mm
Air gap flux density	0.805 T
No. of turns per phase	416

III. MATHEMATICAL MODEL

As shown in Fig.3, the three-phase windings of the stator are denoted as a, b and c with the same winding number. Permanent magnets are mounted on the surface of the disk type rotor, a non-salient rotor is obtained as a result. The motor can be treated as a conventional synchronous motor, only if the field windings are replaced by permanent magnets.

The PM motor can be readily analyzed by assuming that the permanent magnets of the rotor here have been replaced by an equivalent rotor current i_f with the winding number N_f . The waveform of the MMFs produced by the stator phase windings and the equivalent rotor current i_f may be considered as coarse approximation of sinusoidal functions of ϕ_s and ϕ_r , the same as the distribution of the windings [14] [15]. Where ϕ_s and ϕ_r are the angles measured from the a phase stator winding axis and rotational d axis, respectively. Assuming the number of pole pairs is P , their functions are as follows

$$MMF_{as} = -\frac{N_s}{2P} i_{as} \cos P\phi_s \quad (8)$$

$$N_{as} = \frac{N_s}{2} \sin P\phi_s$$

$$MMF_{bs} = -\frac{N_s}{2P} i_{bs} \cos\left(P\phi_s - \frac{2}{3}\pi\right) \quad (9)$$

$$N_{bs} = \frac{N_s}{2} \sin\left(P\phi_s - \frac{2}{3}\pi\right)$$

$$MMF_{cs} = -\frac{N_s}{2P} i_{cs} \cos\left(P\phi_s + \frac{2}{3}\pi\right) \quad (10)$$

$$N_{as} = \frac{N_s}{2} \sin\left(P\phi_s + \frac{2}{3}\pi\right)$$

$$MMF_f = -\frac{N_f}{2P} i_f \cos P\phi_r \quad (11)$$

$$N_{rf} = \frac{N_f}{2} \sin P\phi_r$$

where N_s is the number of turns of equivalent sinusoidally distributed winding in each phase of the stator.

For the winding distribution depicted as Fig.3 (b), the pitch factor $k_p = 1$, the distribution factor $k_d = \cos(\pi/6) = \sqrt{3}/2$, so the winding factor $k_w = k_p \times k_d = \sqrt{3}/2$. Then N_s can be calculated as

$$N_s = \frac{4}{\pi} k_w N_{ph} \quad (12)$$

where N_{ph} is the actual number of turns in series per phase.

The maximum value of the equivalent MMF produced by PMs, MMF_m , is calculated to be

$$MMF_m = \frac{N_f i_f}{2P} = H_m l_m \quad (13)$$

where, l_m and H_m denote the magnet length and the magnetic field intensity when the magnet is shorted by permeable iron. Then the value of $N_f i_f$ can be achieved as

$$N_f i_f = 2PH_m l_m = 2P \frac{B_r l_m}{\mu_r \mu_0} \quad (14)$$

B_r is the remanent flux density for the PMs, μ_r is the relative permeability, and μ_0 is the magnetic permeability of the air with the value $4\pi \times 10^{-7}$.

The effective air gap length between the surfaces of stator and rotor is defined as g , the magnetic flux density B and magnetic flux are shown as below:

$$B = \mu_0 \frac{MMF}{g} \quad \phi = \int_s B ds \quad (15)$$

As an example, let us determine the total flux linkages of the winding due to current flowing only in a winding, leakage inductances are ignored here.

$$\lambda_{as} = \int N_{as}(\phi_s) \phi_{as}(\phi_s) d\phi_s = P \int_0^{\pi/P} \frac{N_s}{2} \sin P\phi_s \quad (16)$$

$$\int_{\phi_s}^{\phi_s + \pi/P} \left[-\frac{\mu_0 N_s (R_o^2 - R_i^2)}{4Pg} \right] i_{as} \cos P\xi d\xi d\phi_s$$

$$L_{as} = \frac{\lambda_{as}}{i_{as}} = L_s = \frac{\mu_0 \pi (R_o^2 - R_i^2) N_s^2}{8P^2 g} \quad (17)$$

where R_o and R_i are the outer and inner radius of the stator.

Similarly, we can get

$$L_{as} = L_{bs} = L_{cs} = L_s \quad (18)$$

$$L_{ff} = \frac{\lambda_f}{i_{as}} = L_f = \frac{\mu_0 \pi (R_o^2 - R_i^2) N_f^2}{8P^2 g} \quad (19)$$

The mutual inductance between the a and f windings is determined by

$$\lambda_{asf} = \int N_{as}(\phi_s) \phi_f(\phi_r) d\phi_s = P \int_0^{\pi/P} \frac{N_s}{2} \sin P\phi_s \int_{\phi_s}^{\phi_s + \pi/P} \left[-\frac{\mu_0 N_f (R_o^2 - R_i^2)}{4Pg} \right] i_f \cos P(\xi - \theta) d\xi d\phi_s \quad (20)$$

In the same way as above, L_{af} , L_{bf} , L_{cf} can be written as

$$L_{af} = \frac{\mu_0 \pi (R_o^2 - R_i^2) N_s N_f}{8P^2 g} \cos P\theta = L_m \cos P\theta \quad (21)$$

$$L_{bf} = \frac{\mu_0 \pi (R_o^2 - R_i^2) N_s N_f}{8P^2 g} \cos(P\theta - 2/3\pi) \quad (22)$$

$$L_{cf} = \frac{\mu_0 \pi (R_o^2 - R_i^2) N_s N_f}{8P^2 g} \cos(P\theta + 2/3\pi) \quad (23)$$

Therefore, the other mutual inductances can be obtained as

$$L_{ab} = L_{ba} = L_{ac} = L_{ca} = L_{bc} = L_{cb} = -1/2L_s \quad (24)$$

Then,

$$\lambda = (\lambda_f \ \lambda_a \ \lambda_b \ \lambda_c)^T = \mathbf{L} \mathbf{i} = \begin{pmatrix} L_{ff} & L_{af} & L_{bf} & L_{cf} \\ L_{af} & L_{as} & L_{ab} & L_{ac} \\ L_{bf} & L_{ba} & L_{bs} & L_{bc} \\ L_{cf} & L_{ca} & L_{cb} & L_{cs} \end{pmatrix} \begin{pmatrix} i_f \\ i_a \\ i_b \\ i_c \end{pmatrix} \quad (25)$$

where \mathbf{L} is the inductance matrix of the motor, the inductances are determined by (18)(19) and (21)-(24).

The inductance expression of (31) can be simplified when they are expressed in terms of $dq0$ variables

$$\begin{bmatrix} \lambda_f \\ \lambda_d \\ \lambda_q \end{bmatrix} = \begin{pmatrix} L_f & 3/2L_m & 0 \\ L_m & 3/2L_s & 0 \\ 0 & 0 & 3/2L_s \end{pmatrix} \begin{bmatrix} i_f \\ i_d \\ i_q \end{bmatrix} \quad (26)$$

The magnetic energy stored may be calculated as

$$W = \frac{1}{2} (i_f \ i_d \ i_q) (\lambda_f \ \lambda_d \ \lambda_q)^T \quad (27)$$

The attractive force F_s can thus be obtained

$$F_s = -\frac{\partial W}{\partial g} = \frac{\mu_0 \pi (R_o^2 - R_i^2)}{16P^2 g^2} \left[N_f^2 i_f^2 + \frac{5}{2} N_s N_f i_f i_d + \frac{3}{2} N_s^2 (i_d^2 + i_q^2) \right] \quad (28)$$

From the Fleming's left-hand rule, the rotating torque T_s can be expressed as

$$T_s = \frac{3}{2} \times P (\lambda_d i_q - \lambda_q i_d) = \frac{3\mu_0 \pi (R_o^2 - R_i^2) N_s N_f}{16Pg} i_f i_q \quad (29)$$

Here, the air gap between the surfaces of the stator and PMs at the equilibrium point is defined as l_g , so the effective air gap

between the stator and rotor at the equilibrium point can be obtained as

$$g_0 = K_c (l_g + l_m / \mu_r) \quad (30)$$

where K_c is the Carter's coefficient, which is approximately equal to 1. Then F_1 and T_1 can be calculated by substituting $g = g_0 + z$, $i_d = i_{d1}$ and $i_q = i_{q1}$ into (28)(29) whereas F_2 and T_2 can be calculated by substituting $g = g_0 - z$, $i_d = i_{d2}$ and $i_q = i_{q2}$ into the same equations, where z is the displacement of the rotor in the vertical direction. The total force and torque are obtained by (1) and (2).

The radial motions of the rotor are restricted by mechanical ball bearings. Therefore, the axial motion of the rotor is independent of radial motion. The dynamic equation of the axial motion of the rotor is

$$mz'' = F + f_z \quad (31)$$

where f_z is the external force in the direction of z-axis, and the gravity is taken into consideration.

The equation of total torque can be rewritten as

$$T = J\theta'' = K_T i_q \quad (32)$$

And

$$\dot{\theta}' = \omega, \quad J\omega' = K_T i_q \quad (33)$$

where J is the moment of inertia, θ is the rotor angle and ω is the rotational speed.

The voltage equations can be written as

$$\frac{d}{dt} i_d = \frac{1}{L_d} v_d - \frac{R_a}{L_d} i_d + \frac{L_q}{L_d} (p\omega_r) i_q \quad (34)$$

$$\frac{d}{dt} i_q = \frac{1}{L_q} v_q - \frac{R_a}{L_q} i_q - \frac{L_d}{L_q} (p\omega_r) i_d - \frac{\lambda_m}{L_q} (p\omega_r) \quad (35)$$

IV. FEM ANALYSIS AND MODEL VERIFICATION

A. Theory

Magnetic fields in PM motors are always associated with transient excitations and nonlinear magnetic materials. The following three Maxwell equations are relevant to transient applications.

$$\nabla \times \vec{H} = \vec{J} = \sigma \vec{E} \quad (36)$$

$$\nabla \times \vec{E} = -\partial \vec{B} / \partial t \quad (37)$$

$$\nabla \cdot \vec{B} = 0 \quad (38)$$

where \vec{H} denotes the magnetic field density, \vec{J} is the electric current density, σ is the conductivity of the dielectric, and \vec{E} is the electric field intensity.

From (36) and (37), we can obtain

$$\nabla \times \frac{1}{\sigma} \nabla \times \vec{H} + \frac{\partial \vec{B}}{\partial t} = 0 \quad (39)$$

The force and torque can be calculated as the derivative of the stored magnetic co-energy W' with respect to a small displacement. The co-energy can be written as

$$W' = \int_V \left[\int_0^B \vec{H} \cdot d\vec{B} \right] dV \quad (40)$$

Then the component of instantaneous force F_s in the direction of the displacement s is

$$F_s = \frac{dW'}{ds} \quad (41)$$

The instantaneous torque T with a small angular rotation displacement θ is represented by

$$T = \frac{\partial W'(i, \theta)}{\partial \theta} / i = \text{const} \quad (42)$$

B. FEM Analysis

The proposed system described in Section II was analyzed using a time-stepping three-dimensional finite element simulator [16]. The mesh shape of analysis model is shown as Fig.5. Only one stator and rotor are implemented in FEM analysis in order to save computational time, yet it is effective to describe the performances of the entire system.

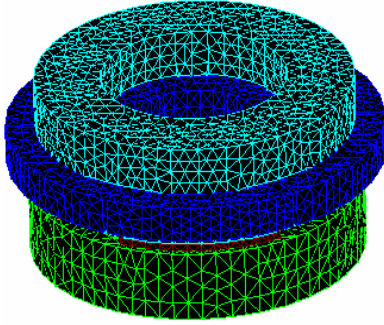


Fig. 5. Mesh shape of analysis model

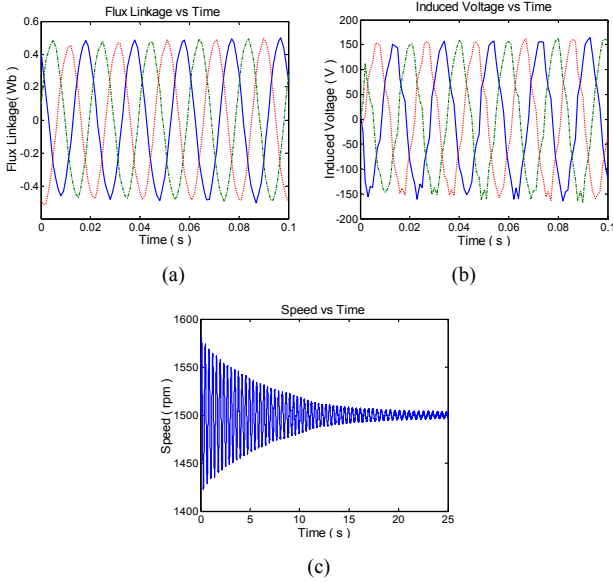


Fig. 6. FEM simulation results when stator fed with 50 Hz sinusoidal current. (a) Flux linkage (b) Induced voltage (c) Rotational speed.

When the stator is fed with 50 Hz sinusoidal current under open-loop condition, and given an initial speed of 1500 rpm, both the flux linkage and induced voltage are quasi-sinusoidal, and the speed settles to the synchronous speed eventually. FEM analysis results are shown as in Fig. 6. It proves that the motor can be analyzed as a sinewave motor, and the mathematical analysis is tenable.

Fig.7 (a) and (b) show the magnetic flux density in the stator and rotor. It is obvious that there are 4 regions having higher flux density in the surfaces of the stator and rotor respectively. It represents 4 poles in the motor. Permanent magnets NdFe35 with the remanent flux density $B_r = 1.23$ T are mounted on the surface of the rotor, so in the region under PMs, the flux density is definitely higher than that at other places.

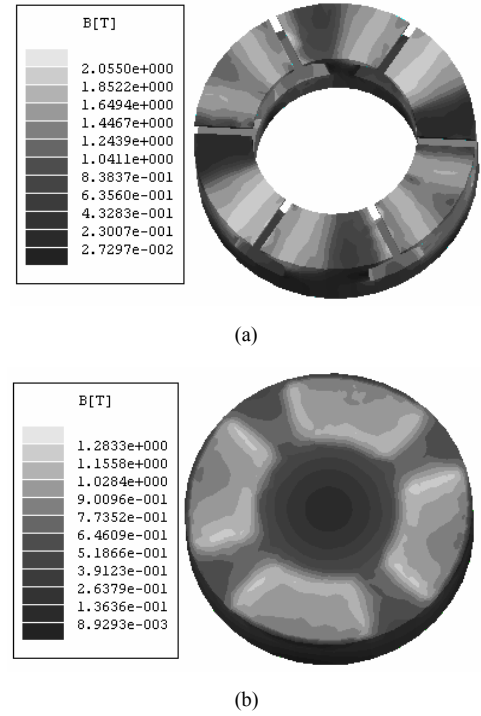


Fig. 7. Magnetic flux distribution of the stator and rotor. (a) Flux density in the stator. (b) Flux density in the rotor.

C. Verification of the Mathematical Model

Three phase currents can be decoupled into dq currents, as shown below

$$i_a = i_d \cos(\theta) - i_q \sin(\theta) \quad (43)$$

$$i_b = i_d \cos(\theta - 120^\circ) - i_q \sin(\theta - 120^\circ) \quad (44)$$

$$i_c = i_d \cos(\theta - 240^\circ) - i_q \sin(\theta - 240^\circ) \quad (45)$$

where θ is the electrical angle of the rotor.

Making $i_q = 0$, we obtain average zero torque as shown in Fig.8 (a). It is evident that the torque has no relations to i_d .

Similarly, assigning $i_d = 0$ and $i_q = 1$, the force, torque and speed can also be obtained as shown in Fig.8 (b)-(d). The force and torque are approximately constant, and the speed increases linearly. It proves that the torque is proportional to i_q .

In this way, by assigning i_q or i_d to zero, and then changing the values of i_d or i_q accordingly, we can get the curves of axial magnetic force and torque at the starting point, as shown in Fig.9. Solid lines represent the calculation results from (28) and (29), and the star marks are the FEM analysis results when it is assigned with different currents. The parameters used in the calculation are listed in Table IV.

TABLE IV
PARAMETERS OF THE PROPOSED SYSTEM

N_s	458 turns
$N_f i_f$	8898 ampere-turns
J	0.0158 kg.m ²
m	4.09 kg
g_0	0.00277 m
R_i	0.038m
R_o	0.065m

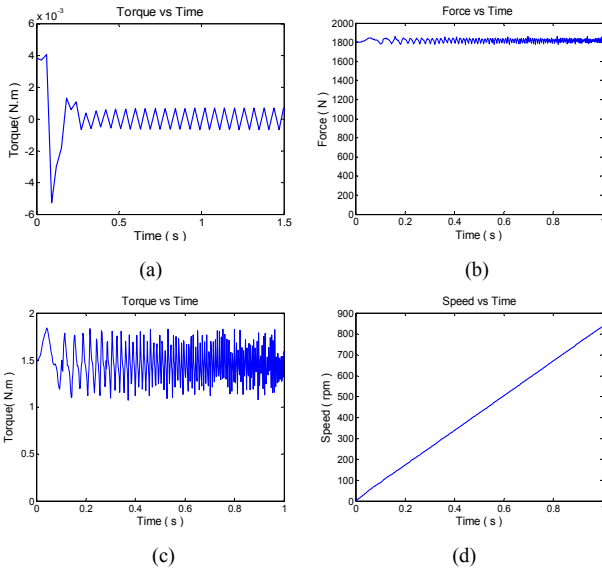


Fig. 8. FEM analysis results when i_q , i_d equals zero respectively. (a) Torque when $i_q = 0$ (b) Force when $i_d = 0$ (c) Torque when $i_d = 0$ (d) Speed when $i_d = 0$.

Fig.9 (a) and (b) show the force and torque when $i_d = 0$ and i_q is changing, Fig.9 (c) and (d) are the cases when $i_q = 0$ and i_d is changing. When $i_q = 0$, the torque is small enough to be regarded as zero. From Fig.9 (b) and (c), we can see that the FEM simulation results correspond to analytical calculation output very well when absolute values of the currents are low.

When they are higher than the maximum rated current which is $1.85 \times \sqrt{2} = 2.62$ A in this design, the force and torque deviate down from the calculation curves. That is caused by the magnetic saturation when high currents are inputted. In Fig. 9 (a), the errors between FEM and mathematical model for small currents still exist. That is because when $i_d = 0$, $N_f^2 i_f^2$ dominates the value of the force shown in (28), a very small error between the $N_f i_f$ values calculated by using (14) and FEM analysis software will cause a large difference for the force values. Fig.9 (e) and (f) show the changes of torque and force when different air-gap lengths are assigned. The results obtained by the two approaches are almost the same.

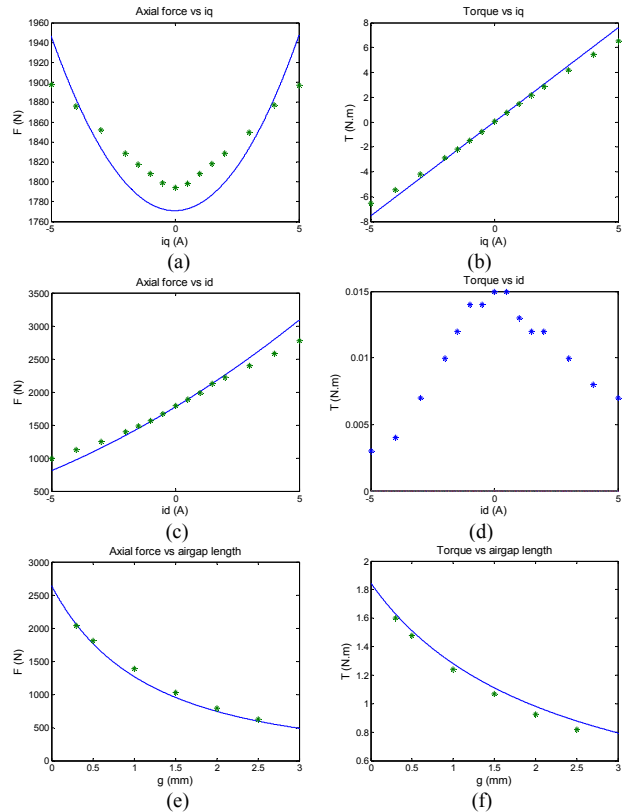


Fig.9. Comparison between FEM simulation results and analytical calculation results.(a) Forces when $i_d = 0$, i_q is changing (b) Torques when $i_d = 0$, i_q is changing (c) Forces when $i_q = 0$, i_d is changing (d) Torques when $i_q = 0$, i_d is changing (e) Forces when $i_d = 0$, $i_q = 1$ and the air-gap length is changing (f) Torques when $i_d = 0$, $i_q = 1$ and the air-gap length is changing.

In order to further verify the accuracy of the mathematical model, Matlab/Simulink can be employed to simulate the performances of the motor, the derived simulation results may then be used to compare with the FEM analysis data.

When the current of $i_d = 0$ and $i_q = 1$ is assigned to the stator windings, the simulation results by Simulink are given in Fig.10. The parameters of the motor in the simulation are as shown in Table IV. By comparing the force and torque curves obtained from Simulink simulation and FEM analysis, which

are shown in Figure 8 (b-c) and Fig. 10 respectively when the same current is assigned, we can see that their average values are quite similar, despite that there are some fluctuations in FEM analysis results.

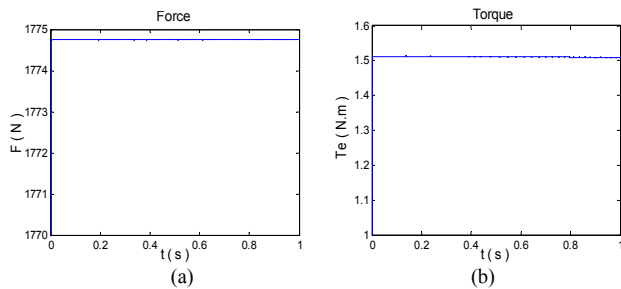


Fig.10. Simulation results by assigning same current i_q to which of Fig.8. (a) Axial magnetic force by Matlab simulation. (b) Torque by Matlab simulation.

Similarly, we can also input the same voltages which are the functions of electrical angle to the motor models in both approaches mentioned above, their results are obtained as shown in Fig. 11. The corresponding curves of force, torque are similar in shapes and values. The results are the evidence that support the accuracy of the mathematical model.

From the FEM analysis results and the comparisons between FEM and simulation results, it is clear that the proposed system is feasible, and the derived mathematical model is accurate and can be used to design drive system.

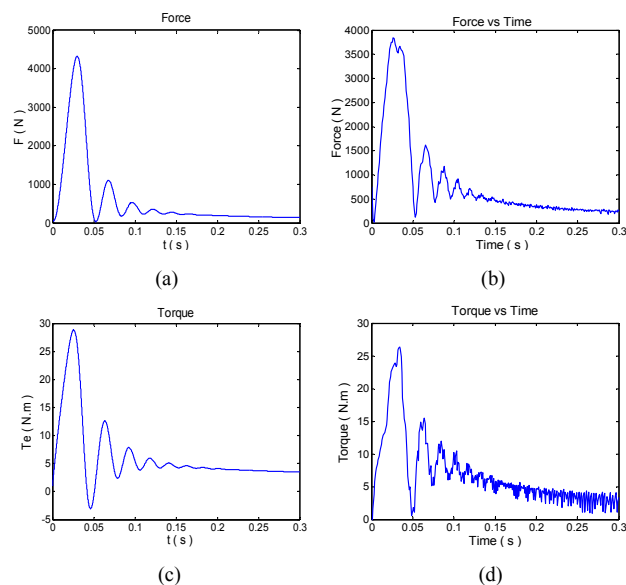


Fig.11. Comparison between Matlab simulation and FEM analysis results by assigning same voltage. (a) Axial magnetic force by Matlab simulation. (b) Axial magnetic force by FEM analysis. (c) Torque by Matlab simulation. (d) Torque by FEM analysis.

V. CONCLUSION

A novel flywheel energy storage system with partially-self-bearing flywheel-rotor has been proposed in this paper. The details of the system structure and design methods were described. Mathematical model has been derived, and 3D

FEM analysis has been conducted to verify the proposed design and mathematical model. All the analysis results obtained supported the feasibility of the proposed system and proved the accuracy of the mathematical model. A prototype of the system is currently under development.

REFERENCES

- [1] R.Beach and D.A.Christopher, "Flywheel technology development program for aerospace applications", *IEEE Aerosp. Electron. Syst. Mag.*, Vol. 13, pp. 9-14, Jun. 1998.
- [2] J.G.Bitterly, "Flywheel technology: past, present, and 21st century projections," *IEEE Aerosp. Electron. Syst. Mag.*, Vol. 13, pp. 13-16, Aug 1998.
- [3] J.Beno, R.Hebner and A.Walls, "Flywheel batteries come around again," *IEEE Spectr.*, Vol. 39, pp. 46-51, Apr. 2002.
- [4] S.Ginter, G.Gisler, J.Hanks, D.Havenhill, W.Robinson and L.Spina, "Spacecraft energy storage systems," *IEEE Aerosp. Electron. Syst. Mag.*, Vol. 13, pp. 27-32, May. 1998.
- [5] H. Kanebako and Y. Okada, "New design of hybrid-type self-bearing motor for small, high-speed spindle", *IEEE/ASME Trans. Mechatron.*, Vol. 8, pp. 111-119, Mar. 2003.
- [6] M.A.Casemore and L.S Stephens; "Actuator gains for a toothless permanent-magnet self-bearing motor", *IEEE Trans. Magn.*, Vol. 35, pp. 4482-4489, Nov. 1999.
- [7] I.da Silva and O. Horikawa; "An attraction-type magnetic bearing with control in a single direction", *IEEE Trans. Ind. Applicat.*, Vol. 36, pp. 1138-1142, Jul./Aug. 2000.
- [8] A. Cavagnino, M. Lazzari and F. Profumo, "Axial flux interior PM synchronous motor: parameters identification and steady-state performance measurements," *IEEE Trans. Ind. Applicat.*, Vol. 36, No.6, pp. 1581-1588, Nov./Dec., 2000.
- [9] A. Cavagnino, M. Lazzari and F. Profumo, "A comparison between the axial flux and radial flux structures for PM synchronous motors," *IEEE Trans. Ind. Applicat.*, Vol. 38, No.6, pp. 1517-1524, Nov./Dec., 2002.
- [10] K. Sitapati and R. Krishnan, "Performance Comparisons of radial and axial field, permanent-magnet, brushless machine," *IEEE Trans. Ind. Applicat.*, Vol. 37, pp. 1219-1226, Sep./Oct.r, 2001.
- [11] S.J. Salon, *Finite Element Analysis of Electrical Machines*, Kluwer Academic Publishers, 1995.
- [12] J. F. Gieras and M. Wing, *Permanent Magnet Motor Technology*, Marcel Dekker, Inc, 2002.
- [13] M.M. Khonsari and E.R. Booser, *Applied Tribology: Bearing Design and Lubrication*. John Wiley & Sons, Inc, 2001.
- [14] A.E.Fitzgerald, C. Kingsley Jr., and S.D.Uman, *Electric Machinery*, 5th edition. New York: McGraw-Hill, 1992.
- [15] P. C. Krouse, O. Wasynczuk and S. D. Sudhoff, *Analysis of Electrical Machinery and Drive System*, 2nd edition. IEEE Press.
- [16] Maxwell 3D Parametric Reference Guide, Ansoft Corporation, 2002.